Functional Studies and Modeling of Pore-Lining Residue Mutants of the Influenza A Virus M2 Ion Channel

ARTICLE *in* BIOCHEMISTRY · DECEMBER 2009

Impact Factor: 3.02 · DOI: 10.1021/bi901799k · Source: PubMed

8 AUTHORS, INCLUDING:

Victoria Balannik
Northwestern University
12 PUBLICATIONS **559** CITATIONS
SEE PROFILE

Vincenzo Carnevale
Temple University
82 PUBLICATIONS **676** CITATIONS
SEE PROFILE

696 *Biochemistry* **2010,** *49,* 696–708
DOI: 10.1021/bi901799k

BIOCHEMISTRY
including biophysical chemistry & molecular biology
Article

Functional Studies and Modeling of Pore-Lining Residue Mutants of the Influenza A Virus M2 Ion Channel†

Victoria Balannik,[‡] Vincenzo Carnevale,[⊥] Giacomo Fiorin,[⊥] Benjamin G. Levine,[⊥] Robert A. Lamb,[§,∥] Michael L. Klein,[⊥] William F. DeGrado,[#,△] and Lawrence H. Pinto*[,‡]

[‡]*Department of Neurobiology and Physiology,* [§]*Department of Biochemistry, Molecular Biology, and Cell Biology,* [∥]*Howard Hughes Medical Institute, Northwestern University, Evanston, Illinois 60208-3500,* [⊥]*Institute for Computational Molecular Science and Department of Chemistry, Temple University, Philadelphia, Pennsylvania 19122-6078,* [#]*Department of Chemistry, and* [△]*Department of Biochemistry and Biophysics, School of Medicine, University of Pennsylvania, Philadelphia, Pennsylvania 19104-6059*

Received October 20, 2009; Revised Manuscript Received December 18, 2009

ABSTRACT: The A/M2 protein of influenza A virus forms a tetrameric proton-selective pH-gated ion channel. The $H_{37}XXXW_{41}$ motif located in the channel pore is responsible for its gating and proton selectivity. Channel activation most likely involves protonation of the H37 residues, while the conductive state of the channel is characterized by two or three charged His residues in a tetrad. A/M2 channel activity is inhibited by the antiviral drug amantadine. Although a large number of functional amantadine-resistant mutants of A/M2 have been observed *in vitro*, only a few are observed in highly transmissible viruses in the presence or absence of amantadine. We therefore examined 49 point mutants of the pore-lining residues, representing both natural and nonnatural variants. Their ion selectivity, amantadine sensitivity, specific activity, and pH-dependent conductance were measured in *Xenopus* oocytes. These measurements showed how variations in the sequence lead to variations in the proton conduction. The results are consistent with a multistep mechanism that allows the protein to fine-tune its pH−rate profile over a wide range of proton concentrations, hypothesized to arise from different protonation states of the H37 tetrad. Mutations that give native-like conductance at low pH as well as minimal leakage current at pH 7.0 were surprisingly rare. Moreover, the results are consistent with a location of the amantadine-binding site inside the channel pore. These findings have helped to define the set of functionally fit mutants that should be targeted when considering the design of novel drugs that inhibit amantadine-resistant strains of influenza A virus.

The M2 protein from influenza A virus (A/M2) forms a proton channel that is essential for virus replication (*1*, *2*). The channel consists of four identical subunits of 97 amino acids; each polypeptide chain has 24 N-terminal extracellular residues, a hydrophobic transmembrane domain of 19 residues, and a 54-residue cytoplasmic tail. Each subunit is a type III integral membrane protein (N_{out}, C_{in}) (*3*). The A/M2 protein forms one of the smallest known *bona fide* ion channels; it is capable of pH-dependent gating and is highly selective of protons vs other ions (*4*−*7*). The highly conserved $H_{37}XXXW_{41}$ gating motif located in the narrow pore formed by the transmembrane (TM) domains of the four subunits is responsible for the channel's proton selectivity and rectification (*8*−*10*). Extensive structural and functional studies suggest that A/M2 channel activation requires a conformational rearrangement of the pore region which involves constriction of the upper vestibule at the level of the V27 residue and relaxation of the pore region at the level of the gating motif (*11*−*13*). Proton flow through the channel most likely involves protonation of the H37 residues (*8*), and solid-state NMR studies performed on the A/M2 transmembrane peptide suggest that the conductive state of the channel is characterized by the tetrad of H37 residues, which alternate between the +2 and +3 state during proton conduction (*10*, *13*−*15*).

The activity of wild-type A/M2 channels is efficiently inhibited by the antiviral drug amantadine (*16*, *17*). Until very recently, the location of the drug-binding site was somewhat controversial. Studies including high-resolution X-ray crystallography of the channel protein indicated that the pore-lining residues are involved in the formation of a binding pocket for amantadine (*11*, *13*, *18*). Solution NMR experiments of the membrane-spanning domain of A/M2 in micelles containing 40 mM rimantadine identified a secondary drug binding site outside of the channel pore, at the level of D44 and R45 residues (*19*, *20*). This binding site is distinct from the pharmacologically relevant site, as assessed by electrophysiological experiments and plaque reduction assays of recombinant virus bearing site-directed mutants of A/M2 (*21*). Most recently, the high-resolution structure of the amantadine-bound form of the channel-forming domain of A/M2 was determined in native phospholipid bilayers using solid-state NMR to detect directly interactions between deuterated amantadine and ^{13}C-labeled amino acids in the protein (*22*). Confirming the previous crystallographic and solid-state NMR measurements (*11*, *13*, *18*), the high-affinity drug-binding site was shown to lie within the pore, surrounded by V27, A30, Ser31, and G34. The peripheral binding site on the surface of the protein was observed only when this amphiphilic drug comprised 5 mol % of bilayer components, and its interaction

†The research was supported NIH Research Grants R01 AI-57363 (L.H.P.), U01 AI-1074571 (L.H.P., W.F.D., R.A.L., and M.L.K.), R01 AI-20201 (R.A.L.), R01 AI-74517 (W.F.D.), and GM56416 (W.F.D.). R.A.L. is an Investigator of the Howard Hughes Medical Institute.

*Address correspondence to this author. Tel: (847) 491-7915.; Fax: (847) 491-5211. E-mail: larry-pinto@northwestern.edu.

 Published on Web 12/22/2009

with the protein appeared to be primarily a consequence of colocalization of the drug and the protein at high concentrations in the same bilayer.

In cell culture, it is possible to select a large number of drug-resistant A/M2 channels, including L26F; V27 to A, S, G, or D; A30 to T, E, or P; S31N; and G34E (*17*, *23*). Each of these mutations involves pore-lining residues (italicized in the sequence) along the N-terminal region of the channel that leads to the outside of the virus.

$$P\mathit{L}_{26}\mathit{V}_{27}VA\mathit{A}_{30}\mathit{S}_{31}II\mathit{G}_{34}ILH_{37}LILW_{41}ILD_{44}RL$$

A subset of these mutations was found in infected patients following treatment with amantadine (*24*), and reverse-engineered viruses harboring a number of different pore-lining point mutations are able to replicate *in vitro* and in a mouse model (*25*). However, many of these mutations give rise to somewhat attenuated viruses that have a tendency to revert in the absence of drug pressure (*23*, *26*) and do not appear to be highly transmissible. Indeed, large-scale sequencing of transmissible viruses from 1918 to 2008 have identified no highly transmissible viruses with mutations at pore-lining residues A30 and G34 (*27*), which project directly into the pore and are proximal to the invariant $H_{37}xxxW_{41}$ motif. S31N has been the predominant amantadine-resistant mutation in H3N2 and more recently in the 2009 H1N1 subtypes (*28*−*31*). V27A and L26F are also frequently present in variants of A/M2 that occur primarily in amantadine-resistant variants of the H1N1 subtype (*27*, *28*, *32*).

Amantadine resistance in currently circulating subtypes is not a consequence of selective pressure from the use of the drug but rather arose spontaneously and sporadically even before the introduction of the adamantane family of drugs (*27*, *28*, *30*−*32*). Amantadine-resistant forms of the virus arise when a drug-insensitive form of A/M2 segregates with other genomic determinants that provide a selective advantage. Because a highly conductive channel would be toxic to the host, the conductance properties of A/M2 appear to be finely tuned to allow the appropriate level of acidification of the viral interior without inducing premature cellular toxicity prior to full assembly and budding of the virus. Moreover, A/M2 acts in concert with the pH-sensitive fusogenic protein, hemagglutinin (HA), which mediates fusion of the viral envelope with the endosomal membrane in a pH-dependent process. The HA's of some strains of influenza A virus are particularly sensitive to acid-induced conformational changes, which can occur prematurely in the late Golgi apparatus. In general, such strains require a variant of A/M2 that is more conductive near pH 6, as is observed in both amantadine-sensitive D44N (*33*) and amantadine-resistant variants with changes at positions 26 and 27 (*23*).

In summary, influenza virus mutates at such a high rate that each pore-lining residue is almost certainly mutated to all 20 amino acids during the course of a pandemic, but only the most fit variants compete effectively. The high mutation rate is reflected in the large number of variants that can be observed *in vitro* and even in infected humans undergoing treatment with amantadine. However, the great majority of these mutants do not appear to be sufficiently fit to persist in the general population. Of the pore-lining residues only positions 26 and 31, at or near the outer vestibule, and D44, at the inner vestibule, are mutated in widely circulating strains of the virus. We hypothesize that this high degree of conservation arises from the fact that a single mutation in a pore-lining residue actually leads to *four* changes within close physical proximity in this homotetrameric protein, leading to significant changes in the pH-dependent activation or conduction of the channel. This finding explains the relative lack of highly fit amantadine-resistant mutants, given the fact that the drug binds to the functionally conserved pore of the channel.

To test this hypothesis, we have examined a panel of 49 mutants of the pore-lining residues. In contrast to previously published works, which concentrated on single pore-lining residues of the A/M2 channel (*4*, *8*, *9*, *21*, *34*), the current study provides a detailed analysis of the contribution of both channel activity and drug sensitivity. Because the magnitude of conduction is a functionally important parameter, we couple electrophysiological analysis with measurements of the levels of expression and native insertion at the level of individual cells, thereby providing the first quantitative evaluation of the magnitude and pH dependence of conduction for a large group of A/M2 mutants. The great majority of the functional drug-resistant variants involve changes to the residues surrounding the experimentally observed drug-binding site in the pore of the channel. Molecular dynamics of selected variants were conducted to investigate the transport mechanism. These calculations support a mechanism of proton flow through the channel by short water wires leading to and from His residues. Overall, the results are particularly important from the perspective of drug design, providing a rationale for the prevalence of certain drug-resistant phenotypes.

MATERIALS AND METHODS

Molecular Biology and in Vitro cRNA Transcription. The cDNA encoding the influenza virus A/Udorn/72 AM2 protein was inserted into the pGEM3 cloning vector (Promega, Madison, WI) for the expression in *Xenopus* oocytes. Point mutations of the pore-lining residues were introduced employing the QuikChange site-directed mutagenesis method. The regions amplified by PCR were verified by double-strand DNA sequencing. In all cases numbering of amino acids starts from the first methionine of the ORF. For expression in oocytes, plasmids were linearized with *Hin*dIII, and capped cRNA was transcribed *in vitro* using T7 RNA polymerase (mMessage mMachine; Ambion, Austin, TX). The quality of transcripts was assessed by agarose gel electrophoresis and ethidium bromide staining and analytical UV spectroscopy.

Heterologous Expression and Electrophysiological Recordings. Stage V−VI *Xenopus laevis* oocytes were prepared as described previously (*35*). Oocytes were injected with 5−10 ng of cRNA in 50 nL/oocyte and assayed 2−3 days later. Two electrode voltage clamp (TEVC) recordings were carried out using TEV-200 (Dagan, Minneapolis, MN) connected to DIGIDATA 1440A and pCLAMP10 (Molecular Devices, Sunnyvale, CA). Oocytes were superfused with Ca^{2+}-free normal frog Ringer (NFR) solution (in mM): 115 NaCl, 2.5 KCl, 1.8 $MgCl_2$, and 15 HEPES for pH 8.5 or 15 MES for pH 5.5. For the ion selectivity measurements Na^+ in the recording solution was replaced by either K^+ or $NMDG^+$. For the anion replacement experiments Cl^- was replaced by $CH_3SO_3^-$. Currents were recorded at −20 mV. Amantadine (100 μM) (Sigma, St. Louis, MO) was applied to inhibit A/M2-induced currents. For the studies of the pH dependence of the A/M2 channel activity the pH of NFR solution was adjusted to the values from pH 5.0 to pH 8.0. Data were analyzed using ORIGIN 8.0 software (OriginLab, Northampton, MA) and KaleidaGraph 4.0 software (Synergy Software, Reading, PA). The pH-dependent conductances were

analyzed by a nonlinear least-squares fit of eq 2 to the data, using the variables r_1, r_2, pK_1, and pK_2 as the adjustable parameters.

Immunofluorescence on Oocytes and Determination of Relative Specific Activity. Individual oocytes expressing wt or mutant A/M2 channels, the membrane currents of which had been studied previously, were washed with ND96 solution and fixed in 2% paraformaldehyde in ND96 (pH 8.5) for 6−12 h at 4 °C. All of the following steps were carried out at 4 °C, and the ND96 solution used lacked $CaCl_2$ and antibiotics. The ND96 solution contained (in mM) 96 NaCl, 2 KCl, 1 $MgCl_2$, and 5 HEPES, pH 7.4. Fixed oocytes were incubated in ND96 containing 2% nonfat milk for 1 h, followed by a 1 h incubation with 14C2 (anti-A/M2) monoclonal antibody (*36*) at 1:500 in ND96 solution containing 2% milk. The oocytes were washed with an ice-cold ND96 solution three times for 10 min and then incubated with Alexa Fluor 546 labeled goat anti-mouse IgG (Molecular Probes, Inc., Medford, OR) at 1:100 in ND96 containing 2% milk for 30 min. Upon the antibody removal, the oocytes were washed with an ice-cold ND96 solution three times for 10 min again. Fluorescence was measured using a PTI Image Master microfluorometer system (Photon Technology International, Birmingham, NJ) with a 20× 0.5 NA objective on an Olympus IMT-2 microscope. About one-half of the surface of each oocyte was imaged using the CCD camera. The excitation wavelength for the Alexa Fluor was 540 nm. Intensity quantifications (in arbitrary units) were made using Image Master 5.0 software (Photon Technology International). Uninjected oocytes were subjected to the same conditions just described as a control for the autofluorescence from the yolk (*37*).

For each oocyte, the whole-cell current (in nanoamperes) measured by TEVC was plotted against the protein expression level detected by immunofluorescence, and the slope of the obtained curve was normalized to that of the wt A/M2 protein. The normalized values represented the relative specific activity of the channel.

Western Blot Analysis. Western blot analysis of the A/M2 wt and mutant proteins was performed under nonreducing conditions as was described previously (*38*).

Classical MD Simulations. Classical molecular dynamics (MD) simulations were performed using a tetramer of the transmembrane helix region (residues 25−46 hereafter referred to as M2TM). Simulations were performed for the wt and five mutants: V27K, A30K, A30F, S31N, and S31F. All mutants were modeled starting from a recent 1.65 Å resolution X-ray structure of the M2TM. The backbone is very similar to the symmetrical "D4" model of M2TM at intermediate pH presented in ref 11, but the resolution of the structure is significantly better, showing water molecules within the channel lumen. On the basis of the calculation of the nitrogen nuclear magnetic shieldings, the pH of crystallization, and the comparison of the computed water density in this structure with the crystallographically resolved structure (Supporting Information Figure S2), we found that the structure under the conditions of our simulation has two charged histidines on nonadjacent positions, and the other two are neutral and in the epsilon-tautomeric state. This protonation state matches the activated +2 state, which is capable of accepting a third proton during proton translation. Coordinates for the mutated side chains were generated with the Mutator plugin of VMD (*39*). M2TM mutants were embedded into a POPC bilayer in a box containing 5707 TIP3P water molecules. The simulations were performed by applying periodic boundary conditions, and the electrostatic interactions were calculated using the particle mesh Ewald (PME) method (*27*) with a real space spherical cutoff of 12 Å and an accuracy threshold of 10^{-6}. Lennard-Jones interactions were cut off at 12 Å. The equations of motion were solved with the velocity Verlet integrator using a time step of 2.0 fs. The lengths of the bonds involving hydrogen atoms were constrained with the SHAKE method (*28*). Energy minimizations and preliminary MD runs of 1 ns for each mutant were performed to equilibrate the systems, in which harmonic restraints were applied to the heavy atoms of the peptide backbone (with a force constant $k = 20.0$ kcal mol^{-1} Å^{-2}), and an isotropic coupling with the Langevin piston was imposed. Production runs were performed at 310.0 K and 1.013 bar using Langevin temperature and Langevin piston pressure coupling schemes, with decay times of 1 and 0.1 ps, respectively. Analysis was performed on trajectories spanning 15−18 ns collected during subsequent MD runs in which all harmonic restraints were released and only the dimension of the box perpendicular to the membrane was allowed to vary. All of the calculations were done using the NAMD software package (*29*) and the CHARMM force field (*30*). Pictures of M2TM structures were generated with VMD (*39*).

RESULTS

A/M2 Channel Pore-Lining Residue Mutants: Surface Expression and Tetramerization. In order to investigate the mechanisms of A/M2 channel activation, proton conductance, and drug sensitivity, 49 mutants of the A/M2 channel pore-lining residues were generated.

To test the expression levels and the stability of the oligomeric assembly of the A/M2 pore-lining residue mutants, oocytes expressing these channels were subjected to Western blot analysis under nonreducing conditions. All of the tested mutants, including those that did not show any channel activity, were efficiently expressed in oocytes. Similar to results obtained for the wild-type (wt) A/M2 channel, species corresponding to monomers, dimers, and tetramers were detected on gels for all of the tested mutants (Supporting Information Figure S1). The dimeric and tetrameric species are stabilized by the formation of native disulfides on the extracellular N-terminal region of the protein. These findings, which rely on the formation of native disulfides in biological membranes, differ from the results of Pielak et al. (*20*), who found the oligomeric stability of peptides bearing amantadine-resistant mutants of the pore-lining residues to be lower than that of the wt peptide (*20*) in micelles based on a covalent cross-linking assay.

Analysis of the Ion Selectivity of A/M2 Channels with Mutated Pore-Lining Residues. Extensive studies have shown that the A/M2 channel is highly selective for protons over other monovalent cations (*5*, *6*). For A/M2 channels expressed either in *Xenopus* oocytes or in cultured mammalian cells the reversal potential (Vrev) determined from the I/V relationship was found to be nearly equal to the H^+ equilibrium potential (E_H) (*5*, *6*). In the current study we measured the reversal potentials of A/M2 channels having mutations in the pore-lining residues. The mutant ion channel proteins were expressed in *Xenopus* oocytes, and their Vrev was compared to that of the wt channel. The Vrev of the highly proton selective wt A/M2 channel did not change significantly when Na^+, the major monovalent cation present in the recording medium, was exchanged with the presumably impermeable *N*-methyl-D-glucamine ($NMDG^+$) cation in the bathing solution (*5*, *6*, *8*, *40*). In our experiments we measured the I/V relationship in the range of −60 to +80 mV at times

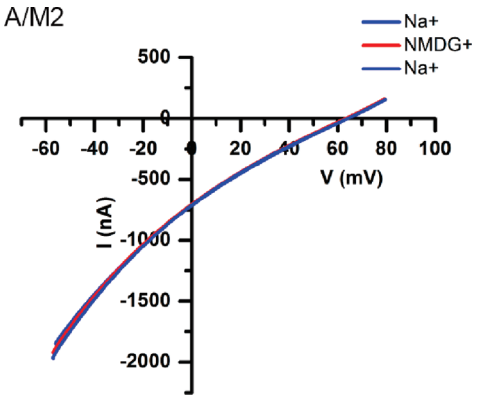

FIGURE 1: A representative trace of the current−voltage relationship (I/V) of wt A/M2 channel activity measured in *Xenopus* oocytes. A/M2 channels were activated by the application of the acidic bathing medium (pH 5.5) for 10 s, and the channel activity was assayed, applying the voltage ramp from −60 to +80 mV to obtain an I/V curve (see Materials and Methods for details). The channel activity was assayed first in the Na^+-based medium (first blue trace). After 3 min recovery at pH 8.5 the channel activity was assayed again in the $NMDG^+$-based medium (red trace), and finally the additional trace of activity was measured in the Na^+-based medium after another 3 min recovery (second blue trace) to ensure that the channel properties and the experimental conditions did not change during the experiment. The I/V curves were plotted after the subtraction of the endogenous oocyte currents recorded at pH 8.5. The Vrev of the A/M2 channels measured in Na^+- or $NMDG^+$-based medium were found to be indistinguishable.

10 and 30 s after activation of the channel by the acidic bathing medium (pH 5.5) (Figure 1). Consistent with previous findings (*6*), no significant difference in the Vrev values was observed between measurements made after 10 and 30 s of acidification. For the analysis of ion selectivity the Vrev values measured after 10 s of acidification were used. In the ion substitution experiments the I/V relationship was measured multiple times on the same oocyte (Figure 1). In order to prevent intracellular acidification a 3 min recovery time was allowed between constitutive acidifications to allow the internal pH of the recorded cell to return to its original value (*6*). Substitution of $NMDG^+$ or K^+ ions for Na^+ in the recording medium did not result in any significant shift in the Vrev of either the wt A/M2 ion channel or the majority of the mutant A/M2 ion channels that contained a mutation at a position N-terminal to the H37 residue (Figure 1 and Supporting Information Table S1). Thus, substitution of amino acids with various properties for outer pore-lining residues, in most cases, did not alter the ion selectivity of the channel.

Replacement of the H37 residue with each of eight amino acids with various properties resulted in the formation of nonselective cationic channels in all cases (Supporting Information Table S1). This finding is consistent with previous observations of the absence of ion selectivity of A/M2 channels carrying the H37G, H37T, H37S, and H37E mutations (*4*, *8*). Anion replacement of Cl^- by $CH_3SO_3^-$ in the recording medium did not result in a significant change in the Vrev of the H37 mutants, indicating the absence of significant anion conductance. Interestingly, most of the mutations of W41 and D44 residues, considered to participate in the A/M2 channel gating (*9*, *11*, *19*), did not produce significant changes in the ion selectivity of the channel (Supporting Information Table S1). However, two mutants of the gating tryptophan residue formed nonselective cationic channels (W41K and W41D, Supporting Information Table S1). Thus, introduction of either a positively or a negatively charged group at position 41 results in the disruption of the ion selectivity of the channel.

Taken together, our results confirm that the ion selectivity of the A/M2 channel is dictated mainly by the H37 residue. No significant changes in ion selectivity can be introduced to the channel by mutating the pore-lining residues located N-terminal of the H37 gate. Thus, mutation of the V27 residue, which has been shown to form the most constricted part of the upper channel vestibule (*11*, *12*, *41*), also does not disrupt ion selectivity. On the other hand, replacement of the W41 residue, which is also known to participate in channel gating, with charged amino acids is capable of disrupting the ion selectivity. Introduction of amino acids with various physical properties at position 44 did not influence ion selectivity. The results above are consistent with a model for proton transport that involves proton binding to the H37 residue (*10*−*12*). The formation of a nonselective cation channel by the introduction of the A30K mutation is of interest and is addressed in the modeling section below.

Analysis of the Amantadine Sensitivity of A/M2 Channels with Mutated Pore-Lining Residues. Wt A/M2 channels are efficiently inhibited by amantadine (*17*). Although the location of the amantadine binding site in the A/M2 protein has been debated recently (*11*, *18*−*21*, *42*), all of the naturally occurring amantadine-resistant influenza A viruses carry mutations in the A/M2 channel pore-lining residues N-terminal to the $H_{37}xxxW_{41}$ gating motif (*17*, *29*, *43*). Here we tested the amantadine sensitivity of the pore-lining residue mutants of the A/M2 protein located either N- or C- terminal of the H37 residue. Mutant channels expressed in *Xenopus* oocytes were activated by acidification (pH 5.5) and exposed to 100 μM amantadine for 2 min. To test the rate of the reversibility of amantadine inhibition, the channel activity was assayed again after the oocyte was bathed in the pH 8.5 solution for 5 min. As expected from the proposed location of the drug in the crystal structure of the protein (*11*), all of the mutants of the residues located N-terminal to H37 position showed altered amantadine sensitivity (Table 1). Amantadine inhibition of recombinant wt A/M2 channels is efficient at low micromolar concentrations (Table 1) (*21*) and reverses only slightly on a time scale of 60−80 min. Among all of the A/M2 mutants located N-terminal to the H37 gate only four (V27W, V27T, S31A, and S31G) exhibited more than 75% inhibition by amantadine at 100 μM (less than 25% residual activity, Table 1). However, even for these cases, the activity remaining after amantadine incubation was 2−3-fold greater than for wt A/M2, indicative of significantly less inhibition of these mutants. Moreover, the rate of amantadine reversibility of these four mutants was significantly faster than that of the wt channel. Thus, both the percent inhibition and the rate of recovery from inhibition were altered by a wide spectrum of mutations to every outer pore-lining residue N-terminal to H37.

Because all of the tested H37 replacement mutants formed nonselective proton channels, we did not measure amantadine sensitivity of these mutants. Of a variety of W41 mutants, W41Y is known to have channel-forming properties very similar to wt (*9*), and this mutant has amantadine sensitivity similar to wt. W41F lacks the electron-rich ring of Trp and Tyr, which has been proposed to be important for maintaining the structure, pH activation, and rectification of A/M2. This mutant as well as W41A had reduced sensitivity to amantadine; it is possible that the reduced sensitivity results from a compromised three-dimensional structure.

Table 1: Summary of Amantadine Sensitivity of A/M2 Pore-Lining Mutants[a]

mutant	activity (%) after inhibition with 100 μM amantadine	SD	activity (%) after 5 min recovery from inhibition	SD
A/M2	6.0	1.4	11.0	2.1
V27A	97.5	4.2	100.0	
V27D	59.1	5.9	100.0	
V27W	13.1	1.9	100.0	
V27G	98.7	6.8	100.0	
V27T	26.5	4.3	100.0	
V27K	60.7	7.6	100.0	
V27S	95.9	3.3	100.0	
V27R	96.1	4.2	100.0	
V27F	NF			
A30D	102.6	6.5	100.0	
A30T	106.0	8.5	100.0	
A30G	82.3	2.2	100.0	
A30F	NF			
A30K	NIS			
S31N	65.4	8.3	95.6	7.2
S31A	17.0	5.2	50.4	0.6
S31G	16.3	1.8	90.2	1.8
S31T	74.0	6.8	93.7	1.6
S31D	64.5	4.4	100.0	
S31K	86.1	20.5	100.0	
S31F	NF			
G34A	72.7	8.4	100.0	
G34E	82.3	9.6	100.0	
G34T	42.0	1.9	36.5	2.1
G34K	102.6	6.5	100.0	
G34F	NF			
G34V	NF			
G34L	NF			
H37A	NIS			
H37S	NIS			
H37G	NIS			
H37K	NIS			
H37N	NIS			
H37F	NIS			
H37D	NIS			
H37Q	NIS			
W41A	42.5	9.8	67.1	3.0
W41G	16.9	5.6	20.5	8.6
W41Y	16.8	0.7	20.8	1.1
W41F	67.3	5.4	81.9	4.4
W41D	NIS			
W41K	NIS			
D44A	13.3	5.3	24.1	1.1
D44K	12.1	4.8	16.0	9.1
D44N	7.0	0.3	19.4	1.5
D44F	11.7	2.5	18.8	1.9
D44G	7.2	0.7	20.8	0.1
D44T	20.3	2.7	22.8	4.3

[a]A/M2 wt and mutant channels expressed in *Xenopus* oocytes were activated by acidification (pH 5.5) and exposed to 100 μM amantadine in the bathing solution (pH 5.5) for 2 min. The remaining channel activity was measured and normalized to the channel activity before the application of the inhibitor. To test the rate of the reversibility of amantadine inhibition, the channel activity was reassayed again after the oocyte was bathed in the pH 8.5 solution for 5 min. The values are the mean (±SD) from measurements from 10−15 oocytes from three to six independent experiments. NF stands for nonfunctional. NIS stands for not ion selective.

The amantadine sensitivity and reversibility of all the mutants of the D44 residue, including the D44N mutant, a naturally occurring variant in the Rostock avian influenza A virus strain (*23*, *33*, *40*), were almost identical to those of the wt A/M2 channel. Mutations of D44 to A, K, N, F, and G failed to have a significant effect on inhibition, while D44T had a tendency to increased residual activity after treatment with 100 μM amantadine (14%). All of the mutants showed slow rates of reversal, similar to that of wt. These results are consistent with the known location of the pharmacologically relevant binding site in the pore of the structure and inconsistent with the hypothesis of amantadine binding to the D44 residue to produce allosteric inhibition as the primary mode of pharmacological inhibition (*19*, *20*) (Table 1).

In summary, amantadine sensitivity was dramatically altered when the pore-lining residues located N-terminal to the H37 gate were mutated. However, for all D44 replacement mutants amantadine sensitivity was found to be similar to that of wt A/M2.

Specific Activity of A/M2 Channels with Mutated Pore-Lining Residues. To compare the activity of a mutant ion channel, containing an altered pore-lining residue, with that of the wt A/M2 channel, the amount of the channel protein expressed on the oocyte surface was assayed by immunofluorescence using an antibody specific to the extracellular N-terminal part of the A/M2 protein (see Materials and Methods). To obtain the relative specific activity, the whole-cell macroscopic conductance for each oocyte was expressed as a function of its protein expression level, and the slope of the curve was normalized to that of the wt channel. The conductance of each channel was measured at pH 5.5, and its specific activity was compared to that of wt at the same pH (Figure 2). The value of pH chosen for the specific activity measurements was pH 5.5, since it is the physiologically relevant pH for A/M2-driven HA activation. Significantly, all mutants of the pore-lining residues located N-terminal to the H37 gate had a decreased specific activity when the residue was replaced with amino acids which maintain the physical properties of the original amino acid but have a larger side chain (Figure 2), as discussed below.

Mutants of the Pore Residues N-Terminal to H37. For V27 two mutations were evaluated that introduce larger hydrophobic side chains, V27F and V27W. While V27F formed a nonconducting channel, V27W had low relative specific activity (Figure 2). The relative specific activities of the mutants with physical properties different from those of the wt channel (for example, V27G, V27T, V27S) are harder to predict, because these changes occur near the end of the helix where it is particularly easy to undergo low-energy conformational deformations in response to changes in sequence.

At position A30 the substitution of the nonpolar aliphatic alanine by the bulkier polar threonine (A30T) resulted in the formation of a channel with a much lower relative specific activity, while the A30F substitution formed a nonconducting channel.

Replacement of the polar uncharged S31 by the larger threonine residue also decreased the channel conductance. The S31N mutant channel had relative specific activity comparable to that of the wt channel (*44*).

G34 replacement by the larger alanine produced a channel with lower specific activity than that of the wt channel, while replacement by residues with even larger side chains (G34L, G34V, and G34F) resulted in the formation of nonconducting channels. The enhanced conductance of the G34T mutant ion channel can be understood from molecular dynamics simulations of the A/M2 channel (*12*, *13*), which shows a critical role for water in the vicinity of the H37. Presumably, the hydroxyl-containing amino acid can aid in creating a path for diffusion of

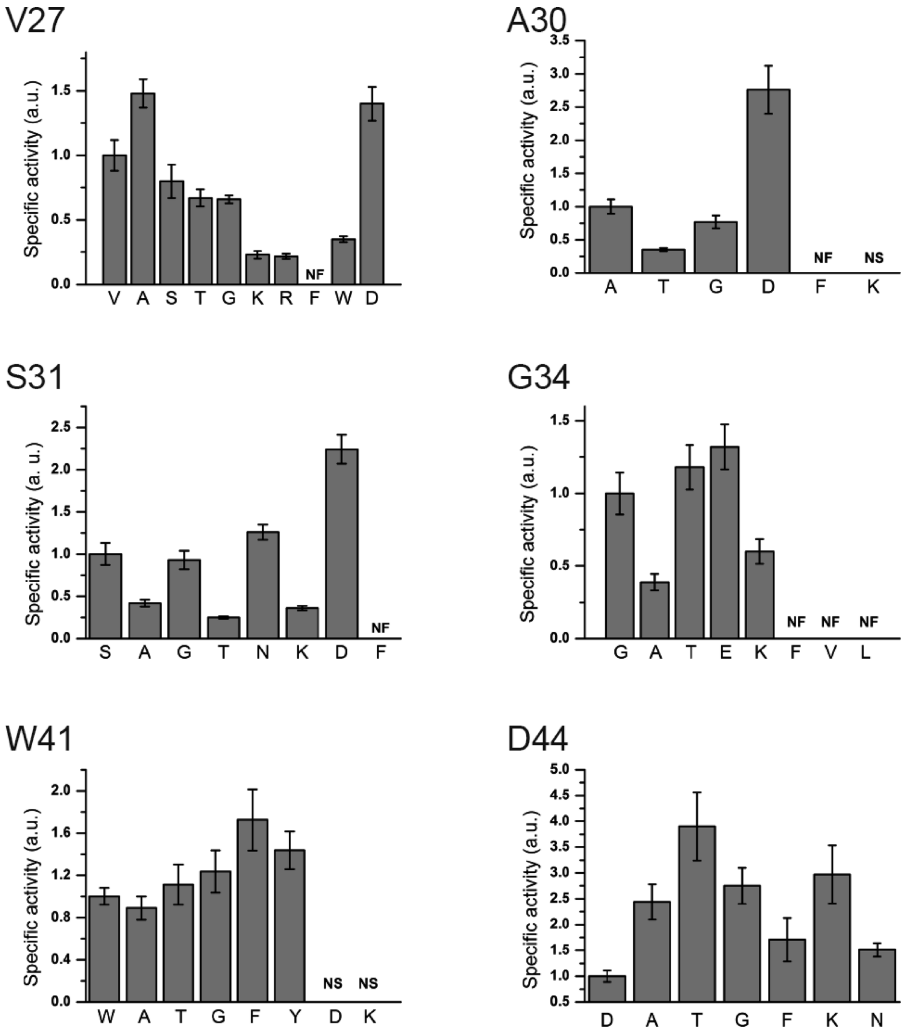

FIGURE 2: Summary of the relative specific activities of the A/M2 mutants with mutations of pore-lining residues. For generating the plots, the amount of channel protein expressed on the oocyte membrane was assayed by immunofluorescence (see Materials and Methods for details), and the whole-cell conductance for each oocyte measured at pH 5.5 was expressed as a function of its protein expression level. The bars represent the slope of the fitted curve, normalized to that of the wt channel. Each bar represents data from 15−20 oocytes and is the mean (±SD) of three independent experiments. NF = nonfunctional channel. NS = nonselective channel.

water/hydronium, while the hydrophobic isostere, Val, is unable to function in this regard.

Substitution of the V27, A30, S31, and G34 residues by the negatively charged aspartate or glutamate in all cases enhanced the conductance of the mutant channels (Figure 2). Because the side chains of Glu and Asp are very polar and easily ionized at acidic pH, the increased relative specific activity may be explained by a variety of causes including the pK_a of the H37 gate (see below), involvement of the acidic residues in proton shuttling, and generalized disruption of the fine-tuned conformational and energetic landscape of the wt A/M2 channel.

Introduction of positively charged residues at positions V27, A30, S31, and G34 decreased the relative specific activity of the proton-selective mutants, possibly due to proton repulsion in addition to effects discussed in the section on molecular dynamics.

Mutants of the Pore-Lining Residues C-Terminal to H37. Interestingly, any mutation of W41 or D44 that resulted in the formation of active and proton-selective channels enhanced the channel conductance (Figure 2). This may be explained by the existence of finely tuned selectivity filter defined by the H37, W41, D44 cluster (*11*, *12*, *19*), which together serve to regulate the pH dependence and magnitude of conductance.

Analysis of the pH-Dependent Activity of A/M2 Channels with Mutated Pore-Lining Residues. One of the goals of this work was to analyze the pH-dependent proton conduction of A/M2 pore-lining mutants in terms of their structures and protonation equilibria. Cross and co-workers (*10*) have examined the protonation of the four H37 A/M2 channel gating residues, which lie within the transmembrane region of the homotetramer. Spectral titrations indicated that the first two imidazoles are protonated with a pK_a near 8 (the signal/noise ratio of the experiment did not allow evaluation of the degree of cooperativity of the transition); pK_a's of the third and fourth H37 residues' protonation are approximately 6 and < 5. Here, we used a similar multiple-protonation scheme to analyze the pH dependence of conduction of this series of mutants. To allow comparison of a large number of mutants, we measured the channel conductance for each mutant in the physiologically relevant direction (inward currents) over the extracellular pH range from 5.0 to 8.0. Although for the pH dependence experiments the channel activity was measured over a wide range of extracellular pHs, the relative specific activity was measured for the most physiologically relevant pH 5.5, which is just above the threshold at which HA causes fusion. Thus, the channel activity obtained from the pH dependence experiments was normalized

to the relative specific activity of each mutant at pH 5.5, which was measured as described above. To minimize voltage-dependent pK_a shifts of H37, the measurements were conducted at low applied voltage (−20 mV).

We assumed that under a constant electrical potential and pH_{in} the observed specific proton current I_{obs} at a given pH_{out} is given by the sum of the products of the mole fraction (f_i) of the channel in each possible protonation state multiplied by the corresponding maximal conductance of that state I_i under the same pH_{in} and electrical potential $I_{obs} = \sum f_i(I_i)$. Thus, the specific activity can be related to the pH_{out} by the equation:

$$I_{obs} = \{I_{max,0} + I_{max,1}[H^+]/K_1 + I_{max,2}[H^+]^2/K_1K_2 + I_{max,3}[H^+]^3/K_1K_2K_3 + I_{max,4}[H^+]^4/K_1K_2K_3K_4\}/\{1 + [H^+]/K_1 + [H^+]^2/K_1K_2 + [H^+]^3/K_1K_2K_3 + [H^+]^4/K_1K_2K_3K_4\} \quad (1)$$

in which K_1 through K_4 are the phenomenological dissociation constants for each successive protonation state of H37, $[H^+]$ is 10^{-pHout}, and $I_{max,i}$ is the associated current of each conductive state.

Negligible conductance is observed at high pH_{out}; thus, we assumed that $I_{max,0}$ can be neglected. Moreover, previous studies indicated that the maximal conductance levels of the A/M2 channel expressed in heterologous systems appear to approach a maximum below pH 5.0 (*5*). The fourth pK_a of the H37 residues is less than 5, so it is unlikely that the quadruply protonated (+4) state is significantly populated by most functional mutants in the pH range of 5−8 explored in occur experiments.

There are three terms remaining in the numerator of eq 1, corresponding to the conductance associated with the +1 through +3 states. The data are not sufficiently precise to allow the definition of the six parameters (I_1 through I_3 and K_1 through K_3) corresponding to these states so we follow the approach proposed by Cross and co-workers (*10*) of treating the first two H37 protonations as a single transition with a unitary cooperativity, leading to the simplified empirical equation:

$$I/I_{pH5.0} = \frac{r_1[H^+]/pK_1 + r_2[H^+]^2/pK_1pK_2}{1 + [H^+]/pK_1 + [H^+]^2/pK_1pK_2} \quad (2)$$

Equation 2 predicts two *phenomenological* protonations with apparent dissociation constants, pK_1 and pK_2, describing the response of the proton flux to pH_{out}. We emphasize that these phenomenological pK values are obtained under kinetic conditions; hence, they might not reflect true equilibrium pK_a values if proton conduction occurs at a rate more rapid than protonation/deprotonation of H37. To allow comparison of mutants with wt, we used a ratio of the channel activity at a given pH to the maximal channel activity obtained at pH 5.0 ($I/I_{pH5.0}$) normalized to the relative specific activity, leading to the parameters r_1 and r_2 in eq 2, which correspond to the maximal conduction of the two states associated with pK_1 and pK_2. In this equation r_1 is a complex relative rate constant; in a complete treatment of the data it would depend on the transmembrane voltage and inner pH as well as the outer pH. It also depends on the relative rate of conduction from C_1 versus protonation of C_1 to generate C_2. Similarly, r_2 represents a relative rate constant reflecting the net rate of proton conduction via the C_2 state. At limiting high proton concentration it reflects the rate-limiting deprotonation of H^+ from H37 (*8*) in the His-mediated proton relay mechanism. However, eq 2 is also consistent with other conduction mechanisms, which postulate that successive protonations of H37 induce conformational changes to allow conduction via water wires (*12*, *14*, *45*). A complete kinetic mechanism and determination of all the rate constants (and their dependence on transmembrane potential) will require extensive measurements at various pH_{in} and pH_{out} as well as transmembrane potentials for the wt protein. These measurements are beyond the scope of the current report and would be prohibitively time-consuming for a large set of mutants. However, by conducting the measurements under constant voltage and pH_{in}, it is possible to observe important differences in the conductance characteristics of the mutant channels, thereby assessing how specific structural and chemical features contribute to activity.

Figures 3 and 4 present the analysis of the pH-dependent activity for each mutant normalized to the relative specific activity and fitted to eq 2. The obtained pK and r values are shown in tables on the right.

Mutants of the Pore-Lining Residues N-Terminal to H37. The analysis of the V27 mutants revealed that two of the mutants, V27A and V27D, have an increased proton conductance over the entire pH range studied (Figure 3A). The behavior of the V27A mutant is of specific interest, since this is one of the most prevalent amantadine-insensitive, naturally occurring mutants of the A/M2 protein (*27*, *43*, *46*). The conductance of this protein is approximately 1.5-fold greater than that of wt over the entire acidic pH range. Fitting of the pH dependence conductances for this mutant showed that the pK_1 of the V27A channel is significantly lower than that of the wt channel and it is accompanied by an increase in the relative conductance (r_1) at the C_1 stage. In comparison, the pK_2 and r_2 values for this mutant remained similar to those of the wt. The large increase in conductance of the V27D mutant near neutral and acidic pH reflects an increase in r_1 and r_2, which might be a consequence of the effects described in the section above. All other V27 mutants tested demonstrated a decrease in conductance at pH 5−6, although some showed increased leakiness to protons near neutral pH, while V27 replacement with T and S resulted in a significant decrease in the pK_1 value, accompanied by an increase in the r_1 value, similar to V27A. The pK_2 and r_2 values for these mutants remained largely invariant. Positively charged residues introduced at the V27 position dramatically decreased the overall channel conductance. Introduction of K or R might electrostatically impede entry of protons, as mentioned above. In addition, the long alkyl portions of their side chains might interact hydrophobically and block the channel.

Similar to V27D, A30D formed a highly conductive channel over all the tested pH range without introducing changes in the pK_a values (Figure 3B). However, the A30T formed a much less conductive channel with a low r_2 value. This finding is consistent with the fact that A30T was less capable than wt of protecting acid-labile forms of HA from undergoing premature conformational changes in the late Golgi (*23*).

The wt A/M2 channel showed a very low conductance associated with pK_1, which is associated with the C_1 state (Figure 3). The most widespread naturally occurring mutants of A/M2, S31N, showed a slight, but significant increase in the channel activity at low pH but even smaller conductance associated with the C_1 state (Figure 3C). Introduction of A or T residues at position 31, which result in the formation of a more hydrophobic environment at this level, resulted in the formation of channels with a decreased activity over the entire pH range

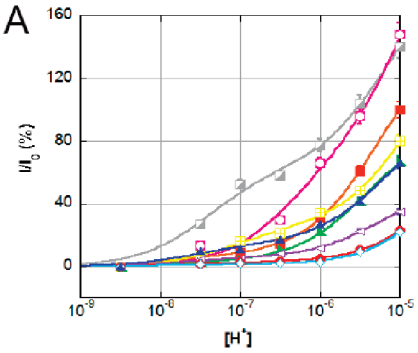

	construct	pK1	pK2	r1	r2	r2/r1
	A/M2	7.8±0.3	5.3±0.1	7.5±1.8	145.3±5.3	19.4
	V27G	7.6±0.4	5.2±0.2	14.9±3.0	98.7±5.4	6.6
	V27R					
	V27W	7.7±0.4	5.3±0.1	5.6±1.3	51.7±4.5	9.2
	V27K					
	V27D	7.4±0.2	5.2±0.3	63.4±8.9	192.2±33.6	3.0
	V27S	7.1±0.2	4.9±0.3	26.6±4.5	157.7±45.9	5.9
	V27A	6.6±0.5	5.1±1.1	59.7±42.9	226.5±87.3	3.8
	V27T	7.6±0.3	5.2±0.1	15.8±6.4	99.7±9.1	6.3

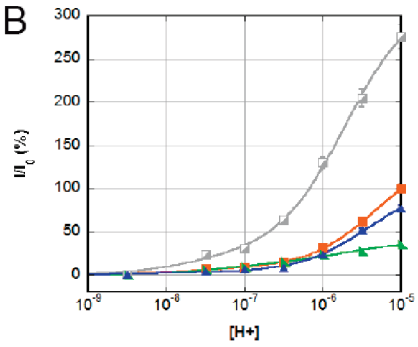

	construct	pK1	pK2	r1	r2	r2/r1
	A/M2	7.8±0.3	5.3±0.1	7.5±1.8	145.3±5.3	19.4
	A30G	8.2±1.8	5.4±0.1	2.8±2.7	105.4±7.3	37.6
	A30D	7.7±0.7	5.7±0.1	25.9±14.1	322.2±11.4	12.4
	A30T	7.3±0.4	5.7±0.3	13.8±2.7	38.8±3.6	2.8

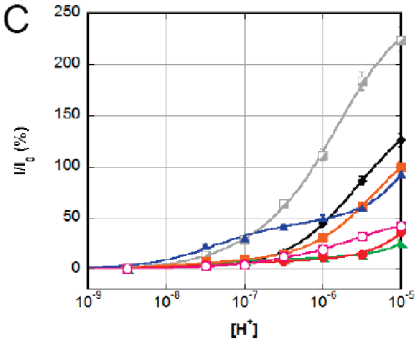

	construct	pK1	pK2	r1	r2	r2/r1
	A/M2	7.8±0.3	5.3±0.1	7.5±1.8	145.3±5.3	19.4
	S31G	7.4±0.1		45±4.1		
	S31D	7.2±0.5	5.8±0.1	35.9±25.7	256.5±7.4	7.1
	S31K					
	S31N	8.0±0.9	5.6±0.3	2.2±5.3	160.8±4.8	74.4
	S31A	6.8±0.5	5.5±0.3	11.7±8.9	51.2±4.0	4.4
	S31T	7.5±0.2		9.8±1.0		

FIGURE 3: Summary of the pH-dependent proton conductance of A/M2 channels with mutated V27, A30, or S31 residues. Left: Channel activity of the pore-lining residue mutants (V27, A; A30, B; and S31, C) was measured in *Xenopus* oocytes in the pH range from 5.0 to 8.0. The channel activity was normalized to the specific activity of each mutant measured at pH 5.5 (see Results and Figure 2). The data were fitted using eq 2. Each point is the mean (±SD) of 10−15 oocytes from three independent experiments. Right: Tables representing the pK_1, pK_2, r_1, and r_2 values (±SD) obtained from the fits on the left using eq 2 (see Results).

studied, while the S31G replacement mutant showed a significant conductance near neutral pH, probably due to the higher H37 deprotonation rate at the C_1 state. Notably, all of the S31 replacement mutants except the naturally occurring S31N showed higher r_1 values than that of the wt channel (Figure 3C), consistent with the greater conductance via the C_1 state. Replacement of S31 with D (which is isosteric with S31N) showed the effect of adding an ionizable group. The S31D mutant exhibited a significantly higher conductance over the tested pH range, which is the result of a shift in the pK_2 and r_2 values associated with the C_2 state to significantly higher levels. Similar to V27K and V27R, the S31K replacement mutant formed a highly disrupted channel, and the pH dependence was not well fitted for these channels using eq 2.

The behavior of the G34 replacement mutants generally resembled that of the replacement mutants at the more outward positions (Figure 4A) and was in good agreement with the implications coming from the channel specific activity measurements discussed above.

Mutants of the Pore-Lining Residues C-Terminal to H37. It was shown that the W41 residue stabilizes charge on H37 via π−cation interactions (*47*). The electron richness of the amino acid aromatic rings follows the series of W > Y > F and, hence, W > Y > F at stabilizing cations. In addition, it was previously proposed that W41 shields the H37 residue on the cytoplasmatic side (*9*). All of the W41 replacement mutants examined in this work introduced smaller residues and hence were probably less able to sterically block access to H37. This property might explain the fact that the W41 replacement mutants showed higher activity over the entire pH range tested (Figure 4B). The mutants had decreased pK_1 values, which may be indicative of lower affinity for protonation in this state (Figure 4B). Normalized r_1 values for the W41 replacement mutants were also significantly increased. This increase followed the expected order of F > Y > W as the electron richness of the aromatic ring and the stability of the H37−W41 interactions decreased.

Similar to W41 mutations, all of the D44 replacement mutants exhibited significantly higher proton conductance over the tested pH range (Figure 4C). D44 was proposed to interact with the A/M2 channel gating residues and thus might be important for gate stabilization (*11*, *19*). Most of the D44 mutants showed higher

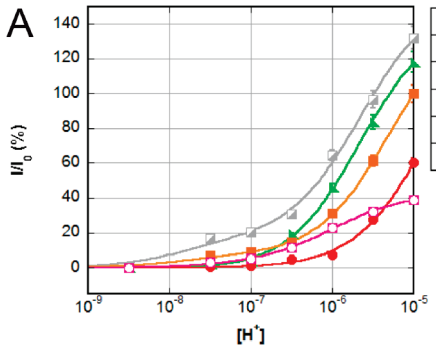

	construct	pK1	pK2	r1	r2	r2/r1
■	A/M2	7.8±0.3	5.3±0.1	7.5±1.8	145.3±5.3	19.4
◪	G34E	7.9±0.7	5.7±0.1	17.7±7.4	156.1±9.1	8.8
●	G34K					
○	G34A	7.7±2.7	6.0±0.1	2.9±3.8	42.4±1.1	14.6
▲	G34T	7.5±4.0	5.7±0.2	3.7±3.3	143.3±5.4	38.7

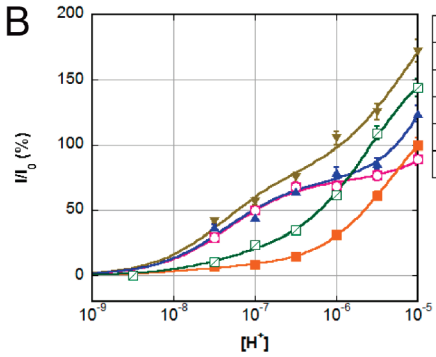

	construct	pK1	pK2	r1	r2	r2/r1
■	A/M2	7.8±0.3	5.3±0.1	7.5±1.8	145.3±5.3	19.4
▲	W41G	7.4±0.2		72.1±6.9		
○	W41A	7.3±0.1		73.4±3.0		
◪	W41Y	7.4±0.4	5.6±0.1	22.4±7.9	176.1±7.2	7.9
▼	W41F	7.4±0.1	5.2±0.1	82.4±12.9	233.1±50.2	2.8

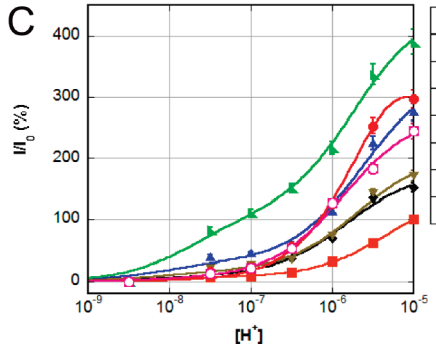

	construct	pK1	pK2	r1	r2	r2/r1
■	A/M2	7.8±0.3	5.3±0.1	7.5±1.8	145.3±5.3	19.4
▲	D44G	8.1±1.2	5.6±0.2	31.9±20.4	339.4±33.8	10.6
●	D44K	8.6±18.3	5.8±0.2	2.2±6.5	354.5±29.4	161.1
▼	D44F	8.1±1.3	5.7±0.2	16.5±12.8	208.4±19.1	12.6
◆	D44N	8.1±2.6	5.8±0.2	9.2±16.6	78.2±14.6	8.5
○	D44A	7.9±3.7	5.8±0.1	8.3±3.3	272.7±4.1	32.9
▲	D44T	7.7±0.4	5.7±0.2	110.8±30.8	449.0±29.6	4.1

FIGURE 4: Summary of the pH-dependent proton conductance of A/M2 channels with mutated G34, W41, or D44 residues. Left: Channel activity of the pore-lining residues mutants (G34, A; W41, B; and D44, C) was measured in *Xenopus* oocytes in the pH range from 5.0 to 8.0. The plots were generated as described in the legend of Figure 3. Each point it a mean (±SD) of 10−15 oocytes from three independent experiments. Right: Tables representing the pK_1, pK_2, r_1, and r_2 values (±SD) obtained from the fits on the left using eq 2 (see Results).

pK_1 and pK_2 values combined with higher levels of r_1 and r_2. Crystallography and NMR studies also showed that the D44 residue might be involved in channel gating in concert with the H_{37}xxxW_{41} gating motif (*11*, *19*).

Molecular Dynamics Investigation of the Effects of Active and Inactive Mutants, V27K and A30K. As discussed above, replacement of the pore-lining residues with large positively charged amino acids like K or R might result in the alteration of the channel activity due to cationic repulsion. Here we compared the properties of the two replacement mutants, V27K and A30K. Despite the fact that the lysine residues are inserted in very similar positions in the two cases (positions 27 and 30 are just one helix−turn apart), V27K was found to be conducting and proton selective (Supporting Information Table S1) with a specific activity at pH 5.5 approximately 25% that of wt (Figure 2), while the A30K mutant formed a nonselective cationic channel (Supporting Information Table S1). In each case the side chain of a lysine residue was inserted within the lumen of the channel in place of a small nonpolar moiety; therefore, electrostatic interactions among the terminal amino group and steric hindrance due to the bulky alkyl part of the side chains might alter the conductive properties of the A/M2. MD simulations shed light on these variations by suggesting differences in the equilibrium structures of these two mutants. MD simulations of the TM region of the protein in a palmitoyloleoylphosphatidylcholine (POPC) bilayer in a box containing 5707 TIP3P water molecules were conducted as described in Materials and Methods.

Figure 5A shows the root mean squared deviation (RMSD) of the C_α atoms of these mutants of the M2TM protein versus the MD simulation time. While the structure of V27K remains stable for the entire trajectory, the structure of A30K changes dramatically over the course of 17 ns, with the RMSD approaching 3 Å.

Given the recently published structures of A/M2 (*11*, *19*, *20*), the difference is readily explained by comparing the two lysine locations. In V27K, the lysines are able to point outside the pore toward the bulk solvent, minimizing the electrostatic repulsion between them. Also, the size of the lumen of the pore is not significantly altered with respect to wt. In A30K, instead, the lysine residues are displaced by one turn of the helix and hence are located deeper inside the channel pore, where their repulsive interactions result in large distortions of the N-terminal portion of the channel from the wt.

Moreover, structural changes in A30K are not limited to the N-terminal end of the channel, but they extend to the H37 tetrad, which plays a major role in determining proton specificity in A/M2. In particular, the mobility of the H37 tetrad is greater in A30K than in V27K (Figure 5). These increased fluctuations reflect a larger ensemble of distinct local geometries of the tetrad: in the wt protein and the functional V27K mutant, H37 side chains are almost constantly oriented such that the vector connecting the two nitrogen atoms of the imidazole ring is perpendicular to the plane of the membrane (Figure 5), similarly to the wt structure; in A30K, instead, a wide variety of structures are observed after 6 ns of MD, including conformations with

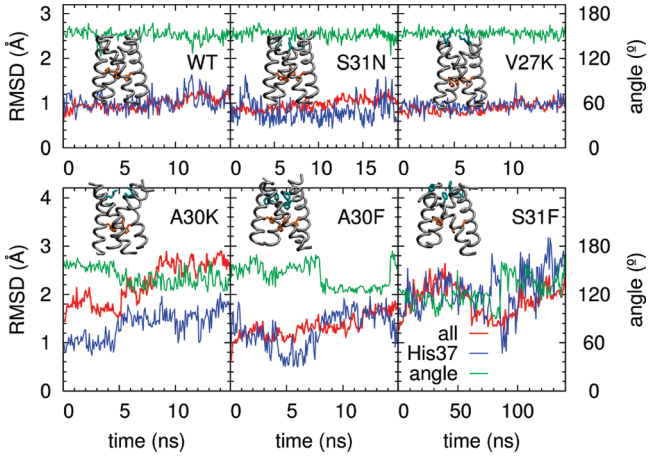

FIGURE 5: Root mean square deviations (RMSDs) of the heavy atoms of M2TM in the MD simulations of the wild-type protein and the mutants S31N, V27K, A30K, A30F, and S31F. Shown are the RMSDs of the whole protein (red) and of the histidine cluster (blue). Snapshots from the dynamics are superimposed to the RMSD plots with gray, cyan, and orange denoting the protein backbone, the mutated side chains, and the H37 side chains, respectively. The angle between the $N_\varepsilon-N_\delta$ vector and the membrane normal for the H37 side chains (averaged over all four histidines) is also plotted as a function of time (green). In the wild-type protein and in the S31N and V27K mutants the histidines remain ordered (RMSD around 1 Å), with the $N_\varepsilon-N_\delta$ vector mostly perpendicular to the membrane plane (the angle is stable around 155°). However, the nonselective A30K mutant and the nonconducting mutants A30F and S31F feature a distorted histidine cluster (RMSD approaching 2 Å or more) and a reduction in the angle with the membrane normal to 120° or less.

$\pi-\pi$ stacking and hydrogen-bonding interactions between adjacent histidines. Arguably, the large-scale disruption of inter-helical and His-His packing leads to a breakdown of the His/Trp selectivity filter, allowing other ions to permeate the channel. Consistently, the water oxygen density profiles depicted in Figure 6A suggest that K27 perturbs the structure of the waters only locally, and the structure of the pore waters appears to be similar to the wt and to the naturally occurring (and thus active) S31N mutant.

Molecular Dynamics Simulations of A30F and S31F, Inactive Mutants of the Pore-Lining Residue. Replacement of each of the tested pore-lining residues located N-terminal of the H37 gate with phenylalanine resulted in the formation of nonconducting channels. A30F and S31F mutants might naively be expected to preserve the wild-type structure given that (1) Phe can be easily accommodated in the pore and (2) this mutation has little effect on the stability of the tetramer (Supporting Information Figure S3) (*48*, *49*). Thus, it seemed reasonable to assume that this mutation might act primarily to alter the structure and dynamics of water in the pore. MD simulations showed that in these mutants the insertion of the benzene moiety induces modest structural changes, but in both of the cases the conductance is expected to be significantly decreased. In A30F, the F30 residues permanently occlude the pore (Figure 6B), and the water density drops to zero in a region roughly the same length of one H-bond (between $z = 5$ Å and $z = 8$ Å; Figure 6B inset), thereby preventing proton transport.

More extensive rearrangements of the protein and water structure are caused by the S31F mutation. Although limited in amplitude (the C_α atoms RMSD is at most 2.5 Å), conformational changes relative to the crystal structure were observed not only near the mutation but also near the H37 and W41 side chains as well (Supporting Information Figure S2). These conformational changes were not complete within the initial 15 ns of the simulations; thus, we continued the MD simulation until a dynamical equilibrium was reached. Two structures were observed to be in equilibrium with one another: a structure indistinguishable from the reported crystal structure and a more open structure, with one or two of the W41 side chains pointing toward the lipids and a wider pore on the C-terminal side. Hence, pore water density profiles computed on different segments of the trajectory vary significantly at the viral inside of the pore, around

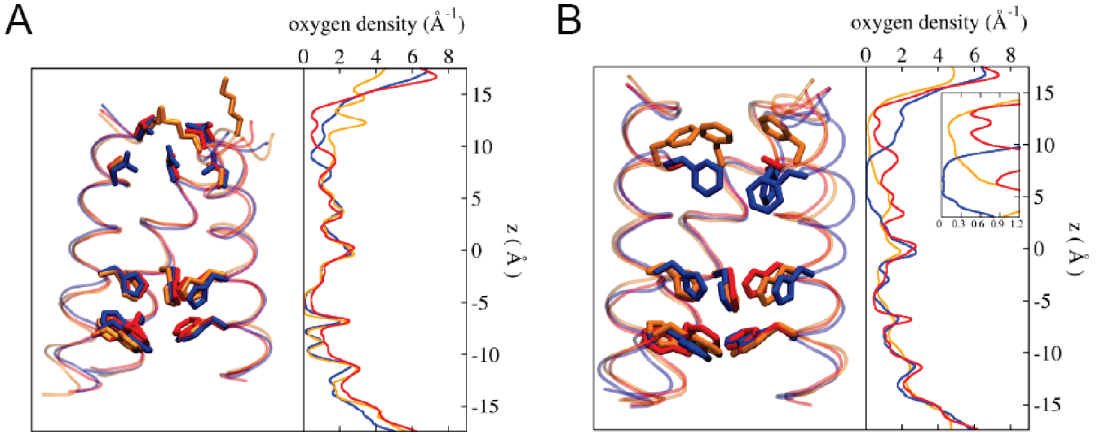

FIGURE 6: The density of water oxygen in the pore as a function of transmembrane displacement (z) is shown along with the structure of the bundle and of selected pore-lining residues (only three chains shown for clarity). In (A) the backbone structure of the wt protein (red) and of the S31N (blue) and V27K mutants (orange) is shown, together with the atoms of the side chains V27, K27, S31, N31, H37 and W41 represented as sticks. In (B), the wt (red), A30F (blue) and S31F (orange) are shown with the side chains A30, F30, S31, F31, H37 and W41. The region of vanishing water density in the mutants A30F and S31F is expanded for clarity.

W41 (see Supporting Information Figure S3). Nevertheless, the water density in the outer section of the pore (where the mutation is located) is fairly stable and negligible in a region extending for one H-bond length (between $z = 9$ Å and $z = 12$ Å); in Figure 6B, we report the density profile computed over the full range of 140 ns.

DISCUSSION

The overall goal of this work was to elucidate the features in the A/M2 sequence that determine the properties necessary for its biological fitness. The evolutionary navigation of sequence space for this channel can be likened to sailing between Scillia and Charybdis; while the virus requires proton conduction to allow RNA uncoating in the endosomal compartment, the facilitation of diffusion of ions across membranes is potentially toxic to the very host cell which the virus relies upon for replication. Thus, the sequence of A/M2 is highly orchestrated to provide high proton selectivity, very low conduction at neutral pH, and the minimal conduction at low pH required for viral replication. Moreover, the fitness of A/M2 depends on the context of the genome of a given virus, including the acid lability of the accompanying hemagglutinin. Here, we demonstrate that A/M2 uses a multistate conduction mechanism to effectively control the conductance characteristics over a wide range of pH in a manner that is exquisitely sensitive to the sequence of A/M2.

Understanding the functional fitness of A/M2 variants will help to define the full spectrum of mutants that should be considered in the design of future inhibitors of A/M2 that address the problem of resistance. Despite the fact that the virus mutates at a great rate and a number of pore-lining mutants can be selected in the presence of amantadine in infected humans, animals, and cell culture, only a handful of variants appear to be permissible in highly transmissible viruses. In particular, most residues that project directly into the channel and are close to the invariant, proton-sensing H37, including A30, G34, and W41, are also invariant in transmissible viruses. We therefore investigated the electrophysiologial properties of a representative set of these and other mutants, including ones that are and are not observed under selective pressure (Supporting Information Table S2). Before discussing these results, however, it is important to discuss the limitations of our measurements. A/M2 is a multifunctional protein, and the acid-induced pH transition might have some secondary influence on another viral function such as fusion (*50*), which our assays would not detect. Furthermore, the A/M2 protein studied here is more efficient at conducting protons down a concentration gradient from the exterior to the interior of the virus than in the reverse direction. This rectification might help to trap protons within a virus or minimize potential toxicities to the host cell that might be encountered if protons were freely allowed to flow in both directions. We measured the conduction in the functionally relevant forward direction, because the reverse measurement is technically impractical when examining a large set of mutants. However, to the extent that the rectifying properties provide a selective advantage, we would not be able to detect this property.

The A/M2 channel consists of an aqueous pore beginning with a constriction at V27 and extending to the proton-selectivity filter at H37. This "outer pore", which connects to the outside of the virus, also comprises the functionally relevant amantadine-binding site (*11*, *13*, *18*, *22*). Indeed, all of the mutants of the outer pore were inhibited significantly less by amantadine than the wt channel (Table 1). V27W, V27T, S31A, and S31G were the only mutants of the outer residues which exhibited amantadine sensitivity at high concentrations of amantadine (100 μM); however, the amantadine inhibition of these mutants was rapidly reversible (Table 1). The C-terminal pore-lining residues form an extended selectivity filter, consisting of H37, W41, and D44. Mutations to the outer pore versus the inner filter have distinctly different effects that we consider separately.

The rate-limiting step in the conduction of protons through the A/M2 channel involves diffusion through (*14*) or dissociation from (*6*) the H37 selectivity filter. Because this represents the bottleneck in inward conduction, mutations to the outer pore will decrease conduction if they either sterically impede proton diffusion to H37 to a rate slower than passage through the selectivity filter or drastically alter the overall structure of the channel. Along these lines, it is interesting to note that all mutations that position a large hydrophobic residue near the conduction pathway (V27F, A30F, S30F, G34V, G34L, G34F) completely disrupt proton conduction (Supporting Information Table S1, Figure 5). These same mutants have not, to the best of our knowledge, been observed in viruses *in vitro* or *in vivo*. Their failure to conduct appears to be due to a loss of function rather than assembly, because the amino acid substitutions do not disrupt either tetramerization as determined by native disulfide formation in cellular membranes (Supporting Information Figure S1) or rigorous thermodynamic measurements in micelles and bilayers (*48*, *49*, *51*). Instead, our MD simulations indicate these large apolar residues snip off water wires required for proton conduction to H37 (Figure 6) and in some cases might also disrupt the geometry of the selectivity filter. Moreover, other conservative mutations that increase the steric bulk of pore-lining residues while maintaining their physical properties tend to decrease conductance as seen in S31T and G34A. However, while small-to-large hydrophobic mutations disrupt conduction, large-to-small mutations do not necessarily increase conductance (e.g., V27G, A30G, S31A, S31G), consistent with previous studies that demonstrated that such mutations can disrupt the three-dimensional structure and or the energetic balance that defines the distribution of conformational states required for efficient gating and conduction (*49*, *51*). Moreover, changing the polarity of the side chains led to more drastic changes in function; introduction of acidic residues (V27D, A30D, S31D, G34D) enhanced conductance even at neutral pH, and introduction of the much larger basic Lys decreased or abolished conductance. MD simulations showed that Lys substitutions more strongly perturbed the conformation of the H37 selectivity filter when it was introduced within the pore versus at the channel entrance, consistent with the properties of the V27K and A30K variants (Figures 5 and 6A).

Mutations to the functionally rich H37-W41-D44 selectivity filter had more uniform effects on function, as every mutant of H37 lost proton selectivity, and every mutant of W41 had a larger conductance than wt (Supporting Information Table S2). W41 is believed to interact with H37, preventing uninterrupted flow of protons through the selectivity filter, particularly in the reverse direction (*9*). Consistent with this expectation, the replacement of W41 with smaller side chains enhanced proton flux. Moreover, the motion and position of W41 appear to be fine-tuned by interactions with D44 (*11*, *19*). Here we show that every mutant of D44 has increased conductance as well as a 0.5 unit shift of pK_2 toward the unperturbed pK_a of histidine, highlighting the importance of this residue in tuning the pH-dependent activation and conductance of the selectivity filter (Supporting Information

Table S2). Finally, it is hardly surprising that most mutations of D44 and W41 had little or no effect on amantadine inhibition, given their distance from the pharmacologically relevant amantadine-binding site within the outer pore.

From a biological perspective it is interesting to note that the only mutants that are observed in highly transmissible viruses (V27A, S31N, D44N) satisfy two conditions: they have channel conductance essentially the same as or up to 1.5-fold higher than that of wt between pH 5.0 and 6.0 *and* they have very low conductances at pH 7 (Figures 3 and 4). With few exceptions (e.g., D44F, A30G, G34T), none of the other variants show this pH-dependent profile of activities. Interestingly, many mutants that have roughly the same conductance as wt at low pH have much greater conductance at neutral pH. Some of these mutations (e.g., V27D, G34E) are formed *in vitro* and *in vivo* under selective pressure from amantadine, although they do not appear in highly transmissible viruses. Thus, the stringent selective pressure associated with formation of highly transmissible viral particles seems to permit only drives toward variants with low levels of conductance at neutral pH.

The multistate conduction of A/M2 might be important to allow a single protein to finely tune its conductance over a wide pH range, thereby providing (1) minimal conduction at pH 7 when the protein is inserted in the cytoplasmic membrane prior to packaging, (2) acidification of the viral interior in the low-pH environment of the late endosome, and (3) protection of HA of certain subtypes in the Golgi under intermediate conditions. We found an excellent fit for all of the mutants to the multistate scheme in eq 2, suggesting that at least two protonation states are able to conduct protons in A/M2. The C_1 state allows a small degree of proton flux near neutral pH. The value of r_2 relative to r_1 defines the magnitude of the conductance near low pH vs at neutral pH. One characteristic of the wt channel is a much greater conductance of the C_2 vs C_1 states ($r_2/r_1 = 19.4$, Figure 3). The pK_a's (pK_1 and pK_2) associated with formation of the two states represent additional parameters that define the pH−conductance curves. It is possible that among the A/M2 mutations found in transmissible influenza viruses (*17*, *29*, *43*) there are significant shifts in both the pK_a's as well as the magnitudes of r_1 and r_2 that might help different strains of the virus adjust to genetic changes in its genome. For example, in strains of the virus that contain a very pH-sensitive variant of HA, A/M2 functions to dissipate the natural acidification of the trans Golgi network. The D44N mutation, which was found to complement this variant of HA (*23*, *33*, *40*), has a significant shift in its pH−conductance curve toward higher pH (Figure 4C), while maintaining minimal conduction near neutral pH. The primary contributors to this shift are an increase in conductance of the C_1 state and an increase in pK_2. The V27A mutation also shows enhanced proton flux arising from an enhanced conductance of the C_1 state ($r_2/r_1 = 3.8$, Figure 3A). By contrast, the most frequently occurring variant, S31N, has a phenotype much closer to that of wt but shows even tighter pH-dependent regulation of conductance than wt, with a value of $r_2/r_1 > 70$ (Figure 3C). V27A as well as S31N is an amantadine-resistant mutant, but current research indicates that the prevalence of these mutations is unlikely to be a function of drug pressure, as there is only a weak selective pressure from amantadine use associated with mutations at V27A and no significant pressure associated with S31N (*27*). Instead, it would appear to be a possibility that the specific pH−flux profiles of these A/M2 proteins are better suited to the specific genetic backgrounds of viruses harboring these variants of A/M2.

In summary, these studies have contributed to the understanding the functional bases for the evolutionary conservation of A/M2. Future design of A/M2 inhibitors can now focus on those mutants that appear most functionally suited to substitute for wt.

SUPPORTING INFORMATION AVAILABLE

The ion selectivity of the A/M2 channels, the protein expression levels, and the supporting modeling data. This material is available free of charge via the Internet at http://pubs.acs.org.

REFERENCES

1. Lamb, R. A., Zebedee, S. L., and Richardson, C. D. (1985) Influenza virus M2 protein is an integral membrane protein expressed on the infected-cell surface. *Cell 40*, 627–633.
2. Pinto, L. H., and Lamb, R. A. (2007) Controlling influenza virus replication by inhibiting its proton channel. *Mol. Biosyst. 3*, 18–23.
3. Pinto, L. H., and Lamb, R. A. (2006) The M2 proton channels of influenza A and B viruses. *J. Biol. Chem. 281*, 8997–9000.
4. Wang, C., Lamb, R. A., and Pinto, L. H. (1995) Activation of the M2 ion channel of influenza virus: a role for the transmembrane domain histidine residue. *Biophys. J. 69*, 1363–1371.
5. Chizhmakov, I. V., Geraghty, F. M., Ogden, D. C., Hayhurst, A., Antoniou, M., and Hay, A. J. (1996) Selective proton permeability and pH regulation of the influenza virus M2 channel expressed in mouse erythroleukaemia cells. *J. Physiol. 494* (Part 2), 329–336.
6. Mould, J. A., Drury, J. E., Frings, S. M., Kaupp, U. B., Pekosz, A., Lamb, R. A., and Pinto, L. H. (2000) Permeation and activation of the M2 ion channel of influenza A virus. *J. Biol. Chem. 275*, 31038–31050.
7. Lin, T. I., and Schroeder, C. (2001) Definitive assignment of proton selectivity and attoampere unitary current to the M2 ion channel protein of influenza A virus. *J. Virol. 75*, 3647–3656.
8. Venkataraman, P., Lamb, R. A., and Pinto, L. H. (2005) Chemical rescue of histidine selectivity filter mutants of the M2 ion channel of influenza A virus. *J. Biol. Chem. 280*, 21463–21472.
9. Tang, Y., Zaitseva, F., Lamb, R. A., and Pinto, L. H. (2002) The gate of the influenza virus M2 proton channel is formed by a single tryptophan residue. *J. Biol. Chem. 277*, 39880–39886.
10. Hu, J., Fu, R., Nishimura, K., Zhang, L., Zhou, H. X., Busath, D. D., Vijayvergiya, V., and Cross, T. A. (2006) Histidines, heart of the hydrogen ion channel from influenza A virus: toward an understanding of conductance and proton selectivity. *Proc. Natl. Acad. Sci. U.S.A. 103*, 6865–6870.
11. Stouffer, A. L., Acharya, R., Salom, D., Levine, A. S., Di Costanzo, L., Soto, C. S., Tereshko, V., Nanda, V., Stayrook, S., and DeGrado, W. F. (2008) Structural basis for the function and inhibition of an influenza virus proton channel. *Nature 451*, 596–599.
12. Khurana, E., Dal Peraro, M., DeVane, R., Vemparala, S., DeGrado, W. F., and Klein, M. L. (2009) Molecular dynamics calculations suggest a conduction mechanism for the M2 proton channel from influenza A virus. *Proc. Natl. Acad. Sci. U.S.A. 106*, 1069–1074.
13. Yi, M., Cross, T. A., and Zhou, H. X. (2009) Conformational heterogeneity of the M2 proton channel and a structural model for channel activation. *Proc. Natl. Acad. Sci. U.S.A. 106*, 13311–13316.
14. Chen, H., Wu, Y., and Voth, G. A. (2007) Proton transport behavior through the influenza A M2 channel: insights from molecular simulation. *Biophys. J. 93*, 3470–3479.
15. Hu, J., Fu, R., and Cross, T. A. (2007) The chemical and dynamical influence of the anti-viral drug amantadine on the M2 proton channel transmembrane domain. *Biophys. J. 93*, 276–283.
16. Sugrue, R. J., Bahadur, G., Zambon, M. C., Hall-Smith, M., Douglas, A. R., and Hay, A. J. (1990) Specific structural alteration of the influenza haemagglutinin by amantadine. *EMBO J. 9*, 3469–3476.
17. Hay, A. J., Wolstenholme, A. J., Skehel, J. J., and Smith, M. H. (1985) The molecular basis of the specific anti-influenza action of amantadine. *EMBO J. 4*, 3021–3024.
18. Cady, S. D., Mishanina, T. V., and Hong, M. (2009) Structure of amantadine-bound M2 transmembrane peptide of influenza A in lipid bilayers from magic-angle-spinning solid-state NMR: the role of Ser31 in amantadine binding. *J. Mol. Biol. 385*, 1127–1141.
19. Schnell, J. R., and Chou, J. J. (2008) Structure and mechanism of the M2 proton channel of influenza A virus. *Nature 451*, 591–595.
20. Pielak, R. M., Schnell, J. R., and Chou, J. J. (2009) Mechanism of drug inhibition and drug resistance of influenza A M2 channel. *Proc Natl Acad Sci U S A 106*, 7379–7384.

21. Jing, X., Ma, C., Ohigashi, Y., Oliveira, F. A., Jardetzky, T. S., Pinto, L. H., and Lamb, R. A. (2008) Functional studies indicate amantadine binds to the pore of the influenza A virus M2 proton-selective ion channel. *Proc. Natl. Acad. Sci. U.S.A. 105*, 10967–10972.
22. Cady, S. D., Schmidt-Rohr, R., Wang, J., Soto, C., DeGrado, W. F., and Hong, M. (2009) Structure of the amantadine binding site of influenza M2 proton channels in lipid bilayers. *Nature* (in press).
23. Grambas, S., and Hay, A. J. (1992) Maturation of influenza A virus hemagglutinin—estimates of the pH encountered during transport and its regulation by the M2 protein. *Virology 190*, 11–18.
24. Shiraishi, K., Mitamura, K., Sakai-Tagawa, Y., Goto, H., Sugaya, N., and Kawaoka, Y. (2003) High frequency of resistant viruses harboring different mutations in amantadine-treated children with influenza. *J. Infect. Dis. 188*, 57–61.
25. Abed, Y., Goyette, N., and Boivin, G. (2005) Generation and characterization of recombinant influenza A (H1N1) viruses harboring amantadine resistance mutations. *Antimicrob. Agents Chemother. 49*, 556–559.
26. Suzuki, H., Saito, R., Masuda, H., Oshitani, H., Sato, M., and Sato, I. (2003) Emergence of amantadine-resistant influenza A viruses: epidemiological study. *J. Infect. Chemother. 9*, 195–200.
27. Furuse, Y., Suzuki, A., and Oshitani, H. (2009) Large-scale sequence analysis of M gene of influenza A viruses from different species: mechanisms for emergence and spread of amantadine resistance. *Antimicrob. Agents Chemother. 53*, 4457–4463.
28. Krumbholz, A., Schmidtke, M., Bergmann, S., Motzke, S., Bauer, K., Stech, J., Durrwald, R., Wutzler, P., and Zell, R. (2009) High prevalence of amantadine resistance among circulating European porcine influenza A viruses. *J. Gen. Virol. 90*, 900–908.
29. Deyde, V. M., Xu, X., Bright, R. A., Shaw, M., Smith, C. B., Zhang, Y., Shu, Y., Gubareva, L. V., Cox, N. J., and Klimov, A. I. (2007) Surveillance of resistance to adamantanes among influenza A(H3N2) and A(H1N1) viruses isolated worldwide. *J. Infect. Dis. 196*, 249–257.
30. Simonsen, L., Viboud, C., Grenfell, B. T., Dushoff, J., Jennings, L., Smit, M., Macken, C., Hata, M., Gog, J., Miller, M. A., and Holmes, E. C. (2007) The genesis and spread of reassortment human influenza A/H3N2 viruses conferring adamantane resistance. *Mol. Biol. Evol. 24*, 1811–1820.
31. Deyde, V., Garten, R., Sheu, T., Smith, C., Myrick, A., Barnes, J., Xu, X., Shaw, M., Klimov, A., and Gubareva, L. (2009) Genomic events underlying the changes in adamantane resistance among influenza A(H3N2) viruses during 2006−2008. *Influenza Other Respir. Viruses 3*, 297–314.
32. Schmidtke, M., Zell, R., Bauer, K., Krumbholz, A., Schrader, C., Suess, J., and Wutzler, P. (2006) Amantadine resistance among porcine H1N1, H1N2, and H3N2 influenza A viruses isolated in Germany between 1981 and 2001. *Intervirology 49*, 286–293.
33. Betakova, T., Ciampor, F., and Hay, A. J. (2005) Influence of residue 44 on the activity of the M2 proton channel of influenza A virus. *J. Gen. Virol. 86*, 181–184.
34. Wang, C., Takeuchi, K., Pinto, L. H., and Lamb, R. A. (1993) Ion channel activity of influenza A virus M2 protein: characterization of the amantadine block. *J. Virol. 67*, 5585–5594.
35. Shimbo, K., Brassard, D. L., Lamb, R. A., and Pinto, L. H. (1996) Ion selectivity and activation of the M2 ion channel of influenza virus. *Biophys. J. 70*, 1335–1346.
36. Zebedee, S. L., and Lamb, R. A. (1988) Influenza A virus M2 protein: monoclonal antibody restriction of virus growth and detection of M2 in virions. *J. Virol. 62*, 2762–2772.
37. Beumer, T. L., Veenstra, G. J., Hage, W. J., and Destree, O. H. (1995) Whole-mount immunohistochemistry on *Xenopus* embryos using far-red fluorescent dyes. *Trends Genet. 11*, 9.
38. Balannik, V., Lamb, R. A., and Pinto, L. H. (2008) The oligomeric state of the active BM2 ion channel protein of influenza B virus. *J. Biol. Chem. 283*, 4895–4904.
39. Humphrey, W., Dalke, A., and Schulten, K. (1996) VMD: visual molecular dynamics. *J. Mol. Graphics 14*, 27–38.
40. Chizhmakov, I. V., Ogden, D. C., Geraghty, F. M., Hayhurst, A., Skinner, A., Betakova, T., and Hay, A. J. (2003) Differences in conductance of M2 proton channels of two influenza viruses at low and high pH. *J. Physiol. 546*, 427–438.
41. Yi, M., Cross, T. A., and Zhou, H. X. (2008) A secondary gate as a mechanism for inhibition of the M2 proton channel by amantadine. *J. Phys. Chem. B 112*, 7977–7979.
42. Ohigashi, Y., Ma, C., Jing, X., Balannick, V., Pinto, L. H., and Lamb, R. A. (2009) An amantadine-sensitive chimeric BM2 ion channel of influenza B virus has implications for the mechanism of drug inhibition. *Proc. Natl. Acad. Sci. U.S.A. 106*, 18775–18779.
43. Bright, R. A., Shay, D. K., Shu, B., Cox, N. J., and Klimov, A. I. (2006) Adamantane resistance among influenza A viruses isolated early during the 2005−2006 influenza season in the United States. *J. Am. Med. Assoc. 295*, 891–894.
44. Stouffer, A. L., Ma, C., Cristian, L., Ohigashi, Y., Lamb, R. A., Lear, J. D., Pinto, L. H., and DeGrado, W. F. (2008) The interplay of functional tuning, drug resistance, and thermodynamic stability in the evolution of the M2 proton channel from the influenza A virus. *Structure 16*, 1067–1076.
45. Wu, Y., and Voth, G. A. (2005) A computational study of the closed and open states of the influenza a M2 proton channel. *Biophys. J. 89*, 2402–2411.
46. Bright, R. A., Medina, M. J., Xu, X., Perez-Oronoz, G., Wallis, T. R., Davis, X. M., Povinelli, L., Cox, N. J., and Klimov, A. I. (2005) Incidence of adamantane resistance among influenza A (H3N2) viruses isolated worldwide from 1994 to 2005: a cause for concern. *Lancet 366*, 1175–1181.
47. Okada, A., Miura, T., and Takeuchi, H. (2001) Protonation of histidine and histidine-tryptophan interaction in the activation of the M2 ion channel from influenza a virus. *Biochemistry 40*, 6053–6060.
48. Howard, K. P., Lear, J. D., and DeGrado, W. F. (2002) Sequence determinants of the energetics of folding of a transmembrane four-helix-bundle protein. *Proc. Natl. Acad. Sci. U.S.A. 99*, 8568–8572.
49. Stouffer, A. L., Nanda, V., Lear, J. D., and DeGrado, W. F. (2005) Sequence determinants of a transmembrane proton channel: an inverse relationship between stability and function. *J. Mol. Biol. 347*, 169–179.
50. Wharton, S. A., Belshe, R. B., Skehel, J. J., and Hay, A. J. (1994) Role of virion M2 protein in influenza virus uncoating: specific reduction in the rate of membrane fusion between virus and liposomes by amantadine. *J. Gen. Virol. 75*, 945–948.
51. Lear, J. D., Stouffer, A. L., Gratkowski, H., Nanda, V., and DeGrado, W. F. (2004) Association of a model transmembrane peptide containing gly in a heptad sequence motif. *Biophys. J. 87*, 3421–3429.